Characterization of Heat Propagation along Single Tin Dioxide Nanobelt Using the Thermoreflectance Method

Xi Wang[1], Younes Ezzahri[1], James Christofferson[1], Yi Zhang[1], Ali Shakouri[1], Li Shi[2], Choongho Yu[3], and Zhong Lin Wang[4]

[1]Electrical Engineering, University of California Santa Cruz, 1156 High Street, Santa Cruz, CA, 95064

[2]Mechanical Engineering, University of Texas Austin, 1 University Station, Austin, TX, 78712

[3]Materials Sciences Division, Lawrence Berkeley National Laboratory, 1 Cyclotron Road, Berkeley, CA, 94720

[4]School of Materials Science and Engineering, Georgia Institute of Technology, 225 North Avenue, Atlanta, GA, 30332

ABSTRACT

In this paper, we studied heat transfer properties of a single tin dioxide nanobelt using non-contact high resolution thermoreflectance imaging technique. Temperature difference across the nanobelt was created by attaching its both ends to a microfabricated thin film heater and sensor pair. High resolution thermal images of the nanobelt and thin film devices were obtained at variant pulsing current amplitudes and frequencies, which allowed us to study the inherent thermal conductance of the nanobelt. Thermoreflectance coefficient change was found to significantly affect the thermoreflectance measurement results.

INTRODUCTION

One-dimensional nanostructures such as nanowires and nanobelts have been studied extensively during the past few years. Compared to bulk materials, in low dimensional inorganic nanostructures, quantum effects and high surface to volume ratio become important. The modified density of electronic states and increased surface scattering, etc, can alter the bulk properties substantially. These significant differences promise one-dimensional nanostructures important applications in the emerging nano-electronic and nano-optical industry. Among all functional nanostructures, the ribbon- or belt- like metal oxide, such as tin dioxide (SnO_2), zinc oxide (ZnO_2) and Indium oxide (In_2O_3) nanostructures are unique due to the reason that they are essentially single-crystalline semiconductors without the presence of a surface insulating layer of native oxides [1].

Thermal transport property is one of the key factors limiting the performance and reliability of all nano-electronic and nano-optoelectronic devices. Metal oxide nanobelts or nanoribbons provide interesting systems for studying heat propagation behavior in low dimension. However, measurement of thermal properties on such small objects is non-trivial. As of today, only a few thermal characterization techniques are able to achieve nanoscale spatial resolution and sub-degree temperature resolution at the same time [2]. Here, we utilized thermoreflectance imaging technique. It is a non-contact temperature measurement technique that eliminates the thermal leakage error accompanied by making thermal contact. We have obtained thermal profiles along a single tin dioxide (SnO_2) nanobelt with various bias currents amplitudes and frequencies applied to the attached micro device.

EXPERIMENT

Sample Details

A belt- like tin dioxide (SnO_2) nanostructure was synthesized using a vapor-solid method [3], [4]. It has a thickness of 450 nm and a width of 230 nm determined by atomic force microscopy and scanning electron microscopy, respectively. The micro device used for external electrical connection and creating temperature gradient across the individual nanobelt was fabricated by the standard micro-fabrication process. It contains two adjacent $14\,\mu$m $\times 25\,\mu$m low stress silicon nitride (SiNx) membranes. Each membrane is supported by five $0.5\,\mu$m-thick, $420\,\mu$m-long and $2.5\,\mu$m-wide low thermal conductivity silicon nitride (SiNx) beams and thermally isolated from the substrate. A 30 nm-thick and 540 nm-wide platinum resistance thermometer (PRT) coil was deposited on each membrane. The PRT was connected to $200\,\mu$m$\times 200\,\mu$m platinum (Pt) bonding pads on the substrate via $1.4\,\mu$m-wide platinum leads on the long SiNx beams. An additional Pt electrode was deposited on each membrane opposite to each other, providing electrical contact to the SnO_2 nanobelt. Figure 1(a) shows a schematic diagram of the micro device structure. The detailed micro-fabrication process can be found elsewhere [1], [5], [6]. Figure 1(b) is a microscopic image of the micro device, which shows the suspended structure and the nanobelt bridging between the two Pt electrodes. The inset of Fig. 1 (a) shows a scanning electron micrograph (SEM) of the tested tin dioxide nanobelt.

To assemble the synthesized nanobelts with the micro device, the nanobelt was first dispersed in an isopropanol (IPA) solution and soaked in an ultrasonic bath for 5 to 10 seconds. Then, the two Pt electrodes in the micro device were connected to an ac voltage source. The solution that contains the nanobelts was dropped on the wafer surface and assembled on the micro device according to a procedure described elsewhere [6]. A focused ion beam (FIB) technique was used to deposit a thin and narrow Pt coating on the contact location between the nanobelt and each electrode so as to improve the electrical and thermal contact [6].

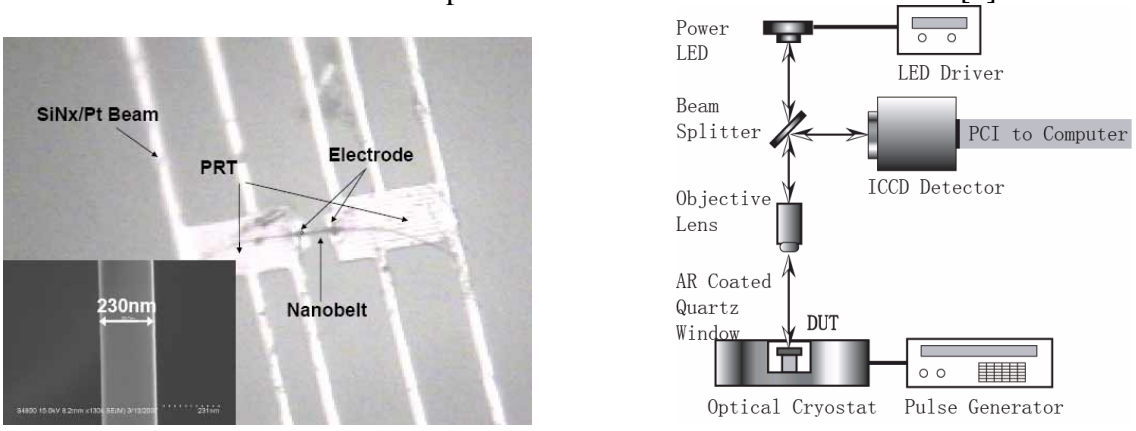

(a) (b)

Fig. 1 (a) .A microscopic image of the micro device with tin dioxide nanobelt bridging between the two Pt electrodes. Inset: Scanning electron micrograph of the tin dioxide nanobelt shows a width of 230nm. (b) An illustration of the thermoreflectance imaging system used in this study.

Thermoreflectance imaging

Thermoreflectance technique is based on the change of the sample surface reflection coefficient as a function of temperature. This small change, about 10^{-4} ~ 10^{-5} range per degree, is typically detected using a lock-in technique when the temperature of the device is cycled [2]. The image object (nanobelt) in this study requires ultra high spatial resolution and sensitivity for low illumination intensity, therefore we chose ICCD as the detection device. Figure 1(b) demonstrates the thermoreflectance imaging setup. Blue light at 455 nm wavelength emitted from a power LED was focused onto the sample through a high magnification objective. The reflected image that contains sample surface temperature change information was projected to an ICCD detector controlled by computer. The sample was kept in an optical cryostat in high vacuum (1~2e-5 torr) to prevent air convection influence on the thermal characterization. While taking the thermal image, pulsed currents with varied amplitude (0~150 μA) and frequency (15~117Hz) were delivered to one side PRT (heating side), and the other PRT (sensing side) was left inactive, so that we could create a temperature difference across the SnO2 nanobelt. A stable ambient temperature of 295 Kelvin was maintained by a thermoelectric cooling (TEC) stage through the experiment.

RESULTS AND DISCUSSION

When supplying current, the heating PRT generated Joule heating in the active SiN_x/Pt membrane. This amount of heat was then divided into two parts: Heating up active membrane (Q_{active}), and heating up the inactive membrane by heat conduction through the SnO_2 nanobelt ($Q_{inactive}$). Radiation and conduction through the residual gas molecules are negligible. The thermal conductance (G_s) of the nanobelt is obtained as

$$G_s = \frac{Q_{inactive}}{\Delta T_h - \Delta T_s} \tag{1}$$

where ΔT_h is the temperature rise at the heating membrane and ΔT_s is the temperature rise at the sensing membrane. Since the two suspended membranes are identical in terms of both material and structure, heat conducted by the SnO_2 nanobelt can be calculated by the equation

$$Q_{inactive} = \frac{\Delta T_s}{\Delta T_h + \Delta T_s} Q \tag{2}$$

Q is the Joule heating generated within the active side PRT and one of the 2 Pt leads used to carry electrical current to the active suspended SiN_x/Pt membrane , which can be calculated using the equation

$$Q = Q_{PRT} + \frac{1}{2} \times 2Q_L = I^2(R_{PRT} + R_L) = IV \tag{3}$$

where R_{PRT} is the electrical resistance of the PRT and R_L is the electrical resistance of one Pt lead. The factor of ½ for heat generation in the two Pt leads origins from the fact that half of the Joule heating produced by each Pt lead is conducted to the heating membrane, while the other half is conducted to the substrate. This has been shown in details in [5]. Therefore, the thermal resistance of SnO_2 nanobelt can be obtained as

$$R_{th} = \frac{\Delta T_h - \Delta T_s}{Q_{inactive}} = \frac{\Delta T_h^{\,2} - \Delta T_s^{\,2}}{\Delta T_s IV} \qquad (4)$$

Thermal images that contain the detailed structure of the micro device and nanostructure were obtained at biasing current 50~150 μ A, 15~117Hz. Figure 2(a) shows the thermal reflectance image of the micro device with the SnO_2 nanobelt bridging between two suspended membranes, when a 150 μ A pulsed current at 65 Hz frequency (7.7 millisecond pulse width) was supplied to the PRT on the active side. Differential electrical resistance method was used to obtain temperature change information at low currents (0~10 μ A).

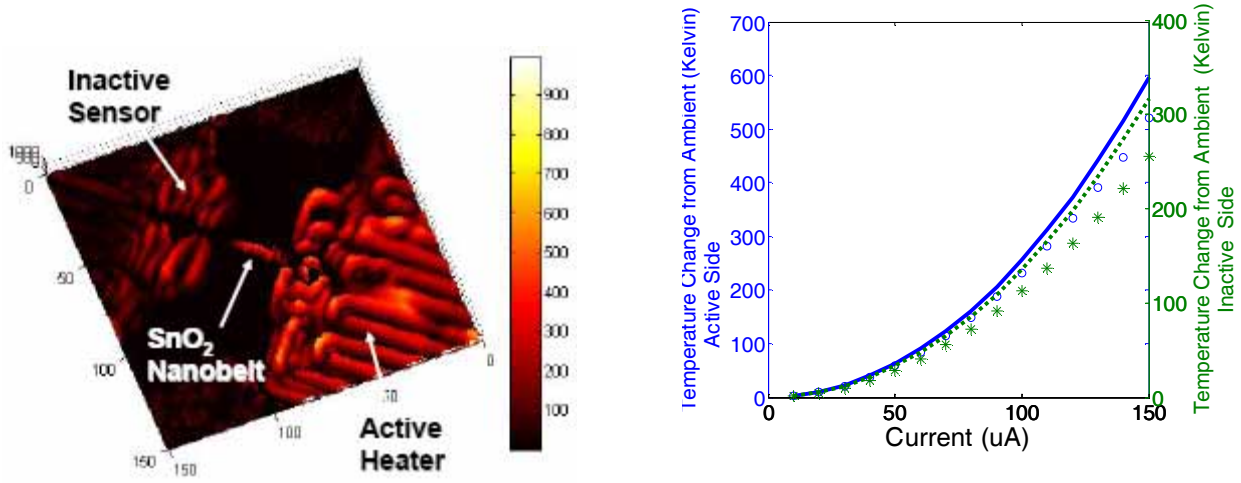

(a) (b)

Fig. 2. (a)Thermoreflectance image and (b) Temperatures rise at heating and sensing sides of the nanobelt versus current. Circle: measured temperature raise (heating side). Cross: measured temperature raise (sensing side). Solid line: calculated temperature rise (heating side). Dashed line: calculated temperatures rise (sensing side).

Measured temperatures of each end of the nanobelt plotted in Figure 2(b) are the average of temperatures over the nanobelt contact area. The calculated temperatures of each end of the nanobelt plotted in Figure 2(b) are obtained based on a thermal resistance network analysis [8]. Good agreement between measurement and calculation was obtain at low currents, while discrepancies were found at high currents. In Figure 3 (a) we plotted the measured nanobelt thermal conductivity at high current (20~150 μ A), which was found to be increasing as the current increasing. In Figure 3 (b) we plotted the measured nanobelt thermal conductivity at low current (0~10 μ A), which shows constancy. The discrepancy between measurement results at high and low currents could be explained as the change of validity of calculation model assumptions. The temperature raises are small ($\Delta T<6K$) at low current (0~10 μ A), so that the heat loss through radiation is negligible, and contact thermal resistance is at least one order of magnitude smaller than the thermal resistance of the nanobelt [1]. However, these assumptions might not be justified at high current. Further, if thermal expansion of the two membranes severely happened at high current, the nanobelt could also experience compression forces from its both ends and its thermal conductivity could also be affected.

Based on the measurement result at small currents (0~10 μ A), the thermal resistance of measured SnO_2 nanobelt was found to be 3.4×10^6 K/W. With the knowledge of sample

dimension, a thermal conductivity of 15.1 W/m/K was derived. This value is significantly lower than the bulk value [7], and comparable to previous measurement results of SnO_2 nanobelt samples [1]. The reduced thermal conductivity was due to increased boundary phonon scatter.

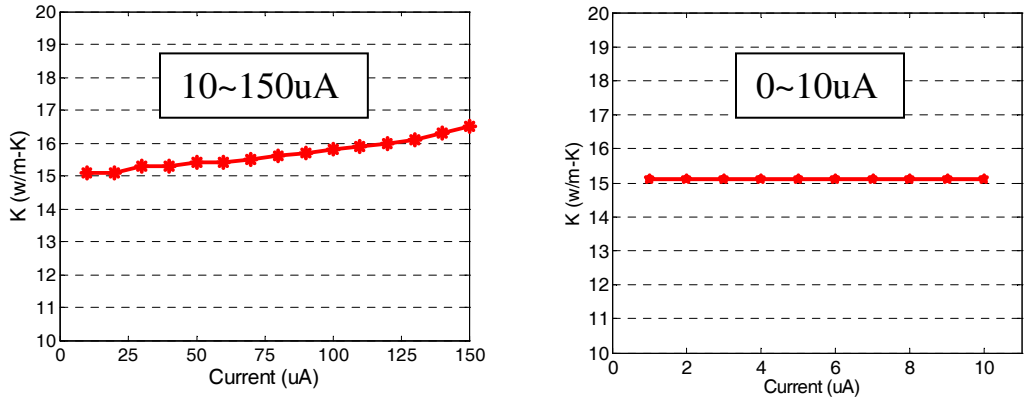

Fig. 3. (a) Measured nanobelt thermal conductivity at high current (20~150 μ A). (b) Measured nanobelt thermal conductivity at high current (0~10 μ A).

Figure 4 shows the temperature change profiles obtained along the SnO_2 nanobelt when varied magnitude current was provided to the active heater. In Figure 4(a) the solid lines represent fitted temperature change profiles based on the temperatures measured on the Pt electrodes. These temperature profiles were fond to agree with Thermal Quadrupoles Modeling results [8], [9], [10]. Points in Figure 4(a) represent the temperature profiles obtained directly from the nanobelt. Note that measured temperature data close to the Pt electrodes are not reliable due to the inevitable edge effect during imaging, and they were not taken into consideration. Solid lines are linear fittings to the directly measured temperature profiles. As one can see, there is a discrepancy between the direct measured nanobelt temperature profile and the fitted temperature profile based on the temperatures measured on each Pt electrode. Further, this discrepancy decreases when lowering the current amplitude. Direct measurement result and indirect prediction show more agreement at lower biasing amplitude. Figure 4(b) shows the distributed thermoreflectance coefficient change along the SnO_2 nanobelt when varied magnitude current was provided to the active heater. Thermoreflectance coefficient changes were estimated using equation (5), where ΔT_f is the fitted temperature profile based on the temperatures measured on each Pt electrode, ΔT_{m} is the direct measured temperature on nanobelt, C_{th} is the thermoreflectance coefficient. i indexes each corresponding points on nanobelt.

$$\left[\frac{\Delta C_{th}}{C_{th}}\right]_i [\%] \approx \left[\frac{\Delta T_{\mathrm{m}} - \Delta T_{\mathrm{f}}}{\Delta T_f}\right]_i [\%] \qquad (5)$$

To explain this distributed thermoreflectance coefficient change, one of the physical mechanisms is thermal expansion. In fact, thermal expansion is proportional to temperature change. Therefore, in a highly heated micro device system, thermal expansion effect could be significant. Further, as the temperature change on the active heater side is much larger than that of the inactive sensor side, more thermal expansion of the suspended membrane occurred on the active heater side. Since the compress forces are linearly dependent on the thermal expansion, the SnO_2 nanobelt experienced more compression near the active heating side. Therefore, the asymmetry of thermoreflectance coefficient change along the nanobelt could also be explained.

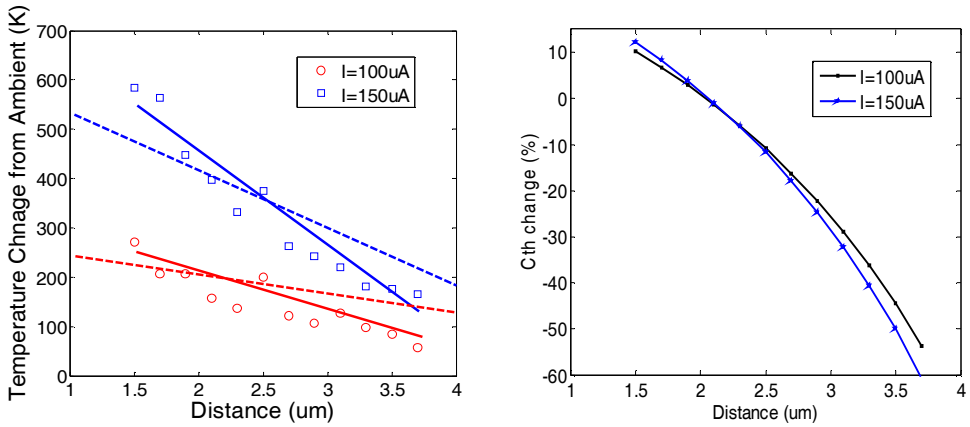

(a) (b)

Fig. 4. (a) Points: measured temperature change profiles along the SnO_2 nanobelt. Solid lines: linear fitting of measured temperature change profiles. Dashed lines: Fitted temperature change profiles based on the temperatures measured on the Pt electrodes. (b) Thermoreflectance coefficient change along the SnO_2 nanobelt.

CONCLUSIONS

We have measured the thermal conductivity of a single SnO_2 nanobelt using a special suspended membrane micro device; the found value was significantly smaller than the bulk value in literature. This agrees with the fact that boundary phonon scattering dramatically increases in nanostructures. We have also shown high resolution thermoreflectance image of the nanobelt and the supporting micro device. Temperature profiles along the nanobelt at varied current amplitude and frequency were obtained, compared and analyzed. We found nano-scale thermoreflectance measurement is highly sensitive and thermoreflectance coefficient can be significantly modified at high current excitation, where thermal expansion effect could play an important role.

REFERENCES

1. L. Shi, Q. Hao, C. Yu, N. Mingo, X. Kong and Z. L. Wang, Appl. Phys. Lett. 84, 2638 (2004).
2. J. Christofferson, K. Maize, Y. Ezzahri, J. Shabani, X, Wang and Ali Shakouri, Proc. of THETA 1(2007).
3. Z. Pan, Z. Dai, and Z. L. Wang, Science 291, 1947 (2001).
4. Z. R. Dai, Z. Wang. Pan and Z. L. Wang, J. Phys. Chem. B 107, 659 (2002).
5. L. Shi, D. Li, C. Yu, W. Jang, D. Kim, Z. Yao, P. Kim and A. Majumdar, J. Heat Transfer, 125, 881(2003)
6. C. Yu, Q. Hao, S. Saha, L. Shi, X. Kong and Z. L. Wang, Appl. Phys. Lett. 86, 063101 (2005).
7. P. Turkes, C. Pluntke and R. Helbig, J. Phys. C: Solid St. Phys. 13 4941-51, (1980).
8. X. Wang, Y. Ezzahri, A. Shakouri, to be submitted.
9. Y. Ezzahri, S. Dilhaire, L. D. Patino-Lopez, S. Grauby, W. Cleays, Z. Bian, Y. Zhang and A. Shakouri, Superlattices and Microstructures, 41, 7-16, (2007).
10. D. Maillet, S. Andre, J. C. Batsale, A. Degiovanni and C, Moyne, Thermal Quadrupoles: Solving the Heat Equation through Integral Transforms, John Wiley & Sons, (2000).